

## Article

# IDA-Based Seismic Fragility Analysis of a Concrete-Filled Square Tubular Frame

Xiaoqiang Liu <sup>1,\*</sup> and Chengxiang Xu <sup>2</sup>

<sup>1</sup> Department of Architectural Engineering, Shandong Vocational College of Science and Technology, Weifang 261053, China

<sup>2</sup> School of Urban Construction, Wuhan University of Science and Technology, Wuhan 430065, China

\* Correspondence: lxq1042@163.com

**Abstract:** Based on the incremental dynamic analysis (IDA) method, this paper conducts seismic fragility analysis of a CFST plane frame, a CFST spatial frame under 1D (one-dimensional) ground motions, and a CFST spatial frame under 2D (two-dimensional) ground motions, with different attacking angles. Firstly, nine-story, three-span CFST frame structures (including the plane frame and spatial frame) were modeled in OpenSees, based on the accurate simulation of the hysteresis performance of the test CFST frames. Then, twenty-five groups of ground motions were employed to analyze the seismic response. Lastly, the IDA curve clusters, probabilistic demand models, and seismic fragility curves of frame structures were researched, respectively. The analytical results showed that the exceeding probability of the spatial frame under 2D ground motions was successively greater than that under 1D ground motions, and greater than the plane frame, and the maximum difference at each performance level was up to 6% and 16%, respectively. The fragility analysis result of the spatial frame was sensitive to the attacking angle of ground motion, and the exceeding probability of the 135°, 150°, and 165° fragility curves was larger than that of the 0° (original attacking angle) fragility curve at each performance level. The research results provide a reference for seismic fragility analysis of CFST frame structures employing the IDA method.

**Keywords:** seismic fragility analysis; CFST frame structure; incremental dynamic analysis (IDA); attacking angle



**Citation:** Liu, X.; Xu, C. IDA-Based Seismic Fragility Analysis of a Concrete-Filled Square Tubular Frame. *Buildings* **2024**, *14*, 2686. <https://doi.org/10.3390/buildings14092686>

Academic Editor: Antonio Formisano

Received: 29 July 2024

Revised: 16 August 2024

Accepted: 26 August 2024

Published: 28 August 2024



**Copyright:** © 2024 by the authors. Licensee MDPI, Basel, Switzerland. This article is an open access article distributed under the terms and conditions of the Creative Commons Attribution (CC BY) license (<https://creativecommons.org/licenses/by/4.0/>).

## 1. Introduction

Catastrophic damage due to earthquakes can cause great loss of livelihood and property. Earthquakes are random and can never be avoided, but damage caused by earthquakes can be prevented or mitigated if preventive measures are taken [1,2]. Several researchers have suggested that probability-based seismic performance design methods should be the mainstream design technique, and seismic fragility analysis is the development and continuation of performance-based design ideas [3,4]. The seismic fragility analysis can evaluate the pre-earthquake hazard of buildings, so that the proposed and constructed structures can be strengthened and repaired in a targeted manner to improve their seismic resistance. It can also provide a basis for post-earthquake structural damage assessment [5]. Several scholars have proposed guidelines and methodologies on the seismic behavior of different structures through fragility analysis, and incremental dynamic analysis (IDA) is considered to be an advantageous technique and the most adopted method, which can investigate the seismic demand capacity under different earthquake intensities [6,7]. Rajkumari summarized the fragility analysis of different building classes and suggested the future scope for fragility analysis of RC structures and transmission towers [2]. In the last two decades, more than half of the fragility analysis research has focused on RC structures, moment-resisting frame structures, and steel frame structures [2], and limited studies on CFST frame structures have been reported to date. With the promotion and application

of CFST structures in high-intensity zones, it is important to conduct fragility analysis for existing or newly designed CFST structures.

At present, the previous studies only focused on the in-plane CFST frame model subjected to 1D ground motions [8,9]. However, each ground motion contains one vertical component and two horizontal components. Taking the ground motion record “RSN3471\_CHICHI.06\_TCU075” as an example in Figure 1, the maximum acceleration of horizontal component E is 1.49 times greater than that of horizontal component N, and the seismic response results of structures are different. Relevant research indicated that the seismic response of a frame structure subjected to 2D ground motions is greater than that subjected to 1D ground motions with the same conditions [10], and the maximum story drift of buildings subjected to 2D ground motions is 1.1–1.3 times greater than that of 1D ground motions [11]. Kostinakis indicated the attacking angle of an earthquake will often have a great impact on the seismic response of the RC structure [12], and Lagaros took the attacking angle of ground motion as an important factor in earthquake probabilistic risk analysis [13]. However, the research on the spatial CFST frame model subjected to 2D ground motions is rare, especially under different attacking angles. Thus, it is necessary to conduct a comparative study on the seismic fragility of the CFST plane frame and spatial frame with the same conditions, and analyze the influence of the attacking angle of ground motions on seismic fragility of the spatial CFST frame.

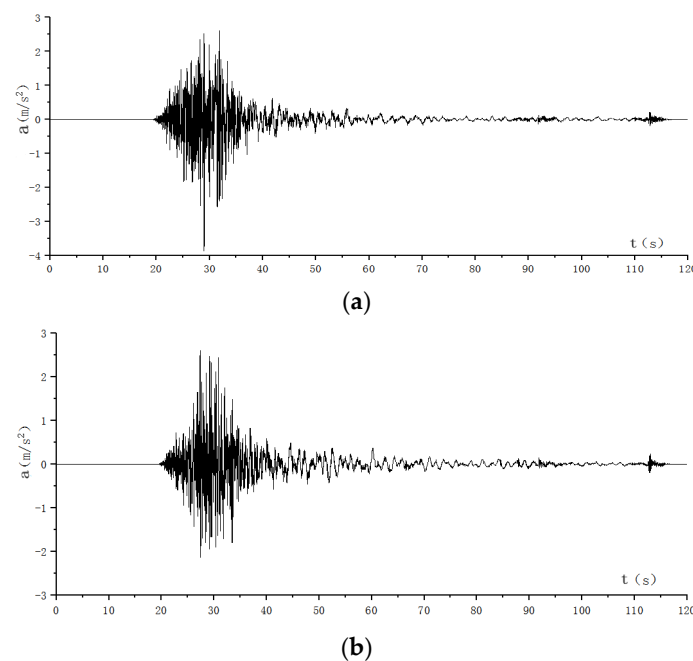


**Figure 1.** Acceleration time histories of “RSN3471\_CHICHI.06\_TCU075”. (a) Horizontal component E. (b) Horizontal component N.

In this paper, typical nine-story, three-span CFST frame structures (including the plane frame and spatial frame) were modeled in OpenSees. According to the seismic fortification intensity, seismic activity characteristics, site conditions, and other conditions, 25 ground motion records were used in the nonlinear dynamic analysis. Furthermore, the IDA-based seismic fragility analysis method was employed to evaluate the seismic performance of the CFST plane frame and spatial frame.

## 2. Structural Modeling of CFST Frames

### 2.1. Structural Design

A typical nine-story CFST frame structure was designed, and the plan view is shown in Figure 2. The total height of the model was 33 m, while the height of the first floor and other floors were 4.2 m and 3.6 m, respectively. The dimensions of steel beams and the CFST

column are listed in Table 1. The thickness of the RC slab was 120 mm, and its concrete grade was C30. The seismic fortification intensity is 8 degrees, and the site is class II. The second o was used for the seismic design. The dead loads and live loads for the floors and roof were 2.0 kN/m<sup>2</sup> and 5 kN/m<sup>2</sup>, respectively, and the gravity loads were considered in beams, columns, and slabs. The CFST frame structure was designed to meet the provisions of the “Technical Code for Concrete-Filled Steel Tubular Structures” (GB50936-2014) and the “Code for the Design of Composite Structures” (JGJ138-2016) [14,15].

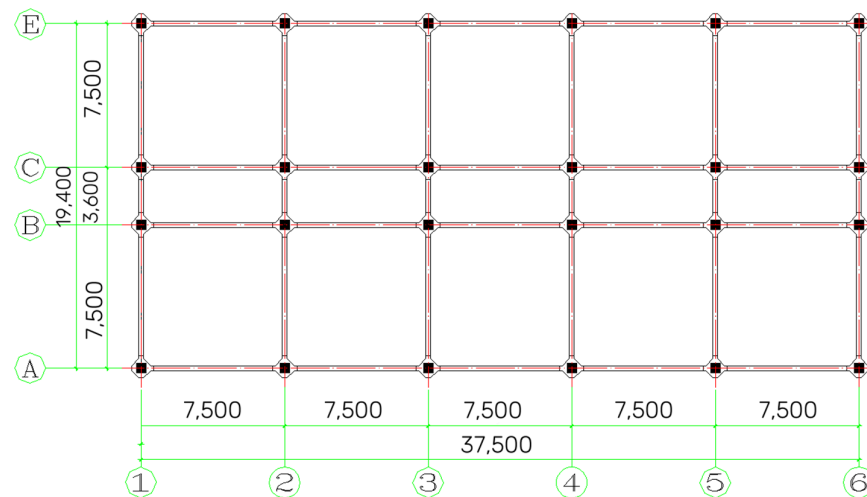


**Figure 2.** Structure plan view (unit: mm).

**Table 1.** The dimensions of steel beams and the CFST column.

Component	Section/mm	Steel Specification	Concrete Strength Grade
Steel beam	H600 × 200 × 8 × 12	Q345	-
	H400 × 180 × 6 × 10	Q345	-
CFST Column	□500 × 500 × 20	Q345	C40

Own research.

## 2.2. Experimental Verification and Modeling Method

The experiment results of the two 2-bay and 3-story test CFST frames tested by our group can be found in [16]. The floor height was 1 m, and the total height reached 3.3 m. The equal-span frame with a span of 1.5 m was denoted as KJE1, while the unequal-span frame with a left span of 2 m and a right span of 1 m was denoted as KJE2. The CFST column showed a cross-section size of 150 mm × 150 mm with a tube wall thickness of 6 mm. The cross-section of the steel beam of KJE1 was H180 × 90 × 6.5 × 10.7, while the cross-sections of the steel beams of KJE2 were H200 × 100 × 4.5 × 7 and H150 × 100 × 6 × 9, respectively. The concrete strength of the CFST columns was C40. The on-site photographs are shown in Figure 3, and hysteretic behavior, failure modes, and other details can be found, if interested, in [16].

OpenSees was used for modeling to simulate the hysteresis behavior of the test frames. The CFST column was simulated using the nonlinear beam–column element, since the cross-sections of the column were kept the same. The beam with hinges element offered in OpenSees could be utilized for simulating frame beams, in which different cross-sections and the existence of bolted connections could be taken into account at the beam ends [17], and the plastic hinge length was determined according to the position of the friction-type bolt at the beam end. The steel was simulated by the Steel02 model. This model, which was implemented by Menegotto and Pinto, was adopted for many types of structural steels in the simulation [18]. Considering the confinement of concrete from the tube, the Concrete02 model was used for the concrete core in the column [17]. The stress–strain relationships of concrete and steel in OpenSees are shown in Figures 4 and 5, respectively.

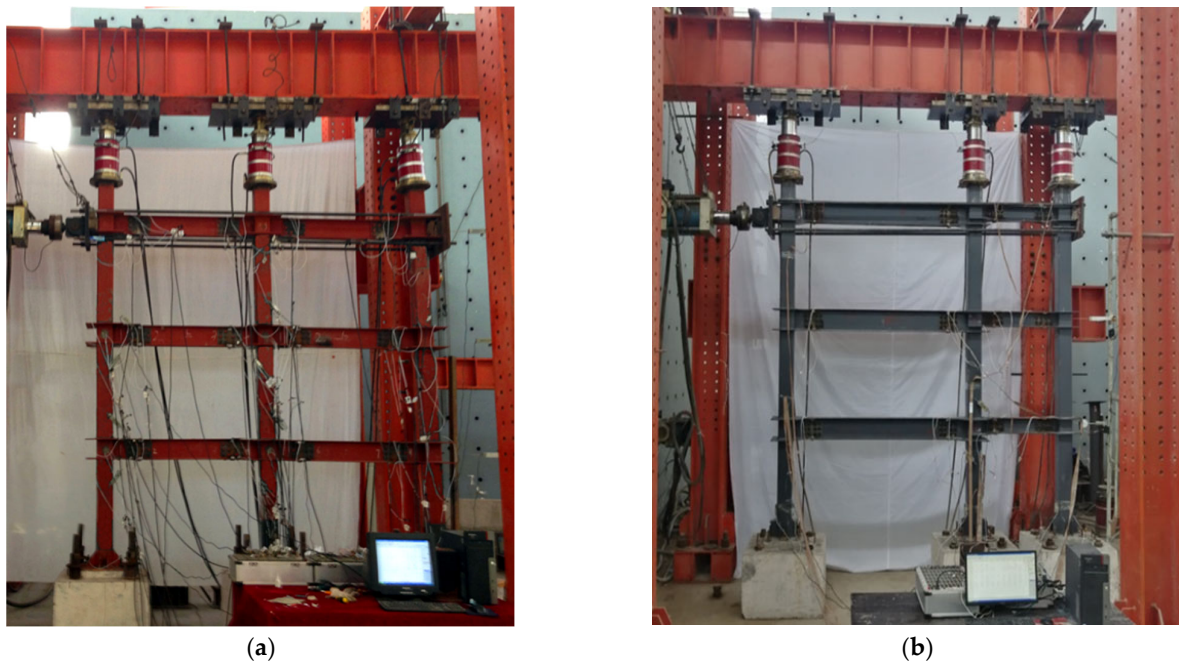


Figure 3. On-site photographs. (a) KJE1 and (b) KJE2.

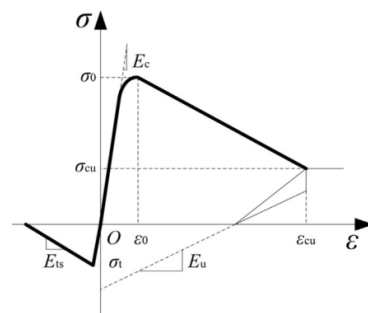


Figure 4. Concrete02 stress–strain curve.

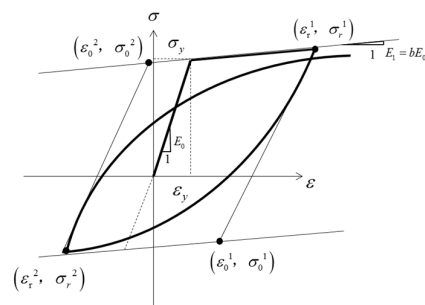
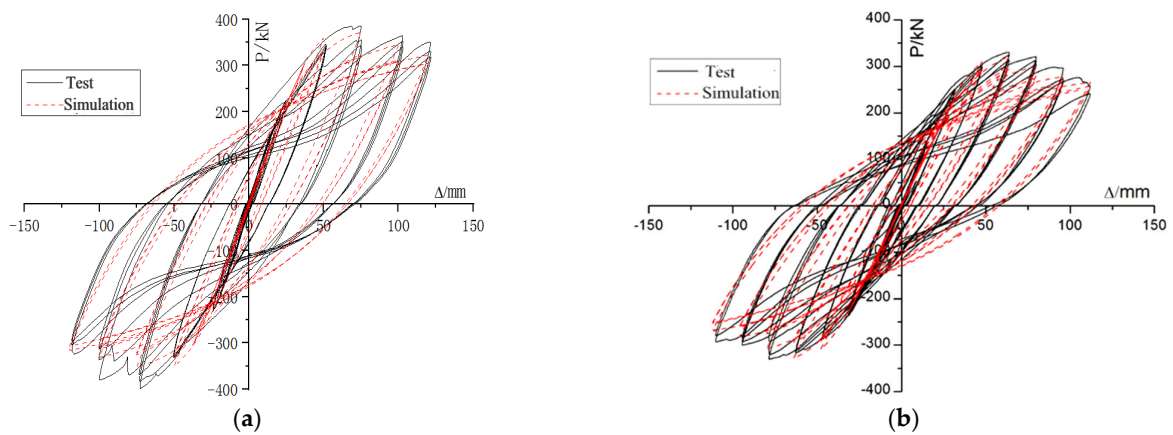


Figure 5. Steel02 stress–strain curve.

The following assumptions were made: (1) a plane section remains planar under loading for beams and columns, (2) bond slip between the steel tube and the concrete is not taken into account, (3) the bending failure occurs before shear failure for members, and (4) no joint failure occurs during the test.

As shown in Figure 6, the shape of the simulated hysteretic curve was similar to that of the test curve. The shapes of the hysteresis curves obtained by numerical simulation were in good agreement with the experimental results, which showed that the adopted modeling method could provide a foundation for further research [19].



**Figure 6.** Comparison of hysteresis curves. (a) KJE1 and (b) KJE2.

### 2.3. Model Establishment

A CFST plane frame model and a CFST spatial frame model were established by OpenSees according to the structural design in Section 2.1, based on the accurate simulation of the hysteresis performance of test CFST frames in Section 2.2, as shown in Figure 7. The steel was simulated by the Steel02 model, and the concrete core in the column adopted the Concrete02 model. Section division of the fiber element of the beam and column is shown in Figure 8. The CFST column was simulated using the nonlinear beam–column element, and the steel beam adopted the beam with hinges element. The modeling method and cross-section properties of each component refer to Section 2.2.

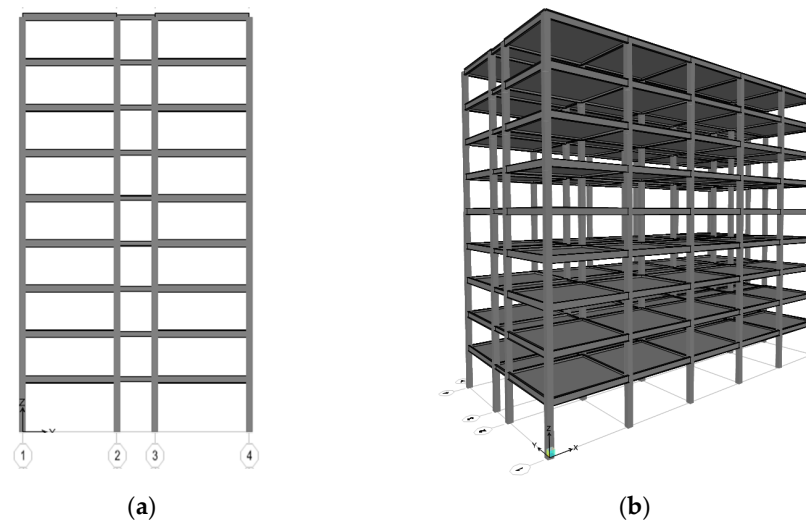


**Figure 7.** Frame models. (a) Plane frame model and (b) spatial frame model.

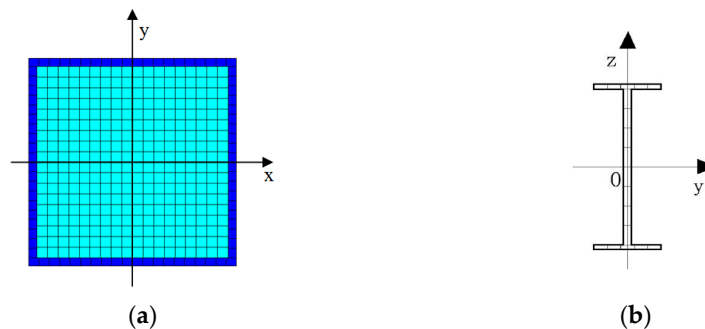


**Figure 8.** Component cross-section. (a) Column and (b) beam.

### 3. Incremental Dynamic Analysis

Incremental dynamic analysis is considered to be an advantageous technique, which can capture the seismic response of the designed frame archetype and evaluate the behavior of structures under different loads of seismicity. Firstly, the amplitude of ground motion is proportionally modulated to different earthquake intensities, and then the corresponding seismic response is recorded by dynamic time history analysis. Finally, the relationship line between IM of ground motions and DM of a structure is the IDA curve.

#### 3.1. Ground Motion Selection

The authors of [4,20] indicated that IDA-based seismic fragility analysis of a mid-high-frame structure can be achieved using 10 to 20 ground motion records. Based on the site conditions (category II) and seismic fortification intensity ( $8^\circ$ ), 25 ground motion records were selected from the Pacific Earthquake Engineering Center (PEER) according to the response spectrum of GB50011-2010 “Code for Seismic Design of Buildings” [21], and the magnitude of the selected records was greater than 5.6 M. The information of ground motion is shown in Table 2: each ground motion record contains 2 horizontal components, and the 25 selected ground motions contain 25 motions in the X direction and 25 motions in the Y direction, named 25N and 25E, respectively.

**Table 2.** Selected ground motions.

Record	Earthquake Name	Year	Platform	$M_w$	Ground Motion Horizontal Component, N/E
1	“Hollister-01”	1961	Hollister City Hall	5.6	RSN26_HOLLISTR_B-HCH181/271
2	“San Fernando”	1971	Santa Felita Dam (Outlet)	6.61	RSN88_SFERN_FSD172/262
3	“Imperial Valley-06”	1979	“Cerro Prieto”	6.53	RSN164_IMPVALL.H_H-CPE147/237
4	“Irpinia_Italy-01”	1980	“Bisaccia”	6.9	RSN286_ITALY_A-BIS000/270
5	“Chalfant Valley-02”	1986	“Long Valley Dam (Downst)”	6.19	RSN553_CHALFANT.A_A-LVD000/090
6	“Chalfant Valley-02”	1986	“Long Valley Dam (L Abut)”	6.19	RSN554_CHALFANT.A_A-LVL000/090
7	“Loma Prieta”	1989	Coyote Lake Dam—Southwest Abutment	6.93	RSN755_LOMAP_CYC195/285
8	“Manjil_Iran”	1990	Abbar	7.37	RSN1633_MANJIL_ABBAR-L/T
9	“Cape Mendocino”	1992	Fortuna—Fortuna Blvd	7.01	RSN827_CAPEMEND_FOR000/090
10	“Cape Mendocino”	1992	Loleta Fire Station	7.01	RSN3750_CAPEMEND_LFS270/360
11	“Landers”	1992	North Palm Springs Fire Sta #36	7.28	RSN3757_LANDERS_NPF090/180
12	“Chi-Chi_Taiwan”	1999	“TCU075”	7.62	RSN3471_CHICHI.06_TCU075 E/N
13	“Duzce_Turkey”	1999	“Lamont 1061”	7.14	RSN1614_DUZCE_1061-N/E
14	“Chi-Chi_Taiwan-06”	1999	“TCU075”	6.3	RSN3471_CHICHI.06_TCU075N/E
15	“San Simeon_CA”	2003	San Antonio Dam—Toe	6.52	RSN4013_SANSIMEO_36258021/111
16	“Chuetsu-oki_Japan”	2007	“Kawaguchi”	6.8	RSN4869_CHUETSU_65042NS/EW
17	“Chuetsu-oki_Japan”	2007	“Ojiya City”	6.8	RSN4882_CHUETSU_65321NS/EW
18	“Chuetsu-oki_Japan”	2007	“NIG024”	6.8	RSN5270_CHUETSU_NIG024NS/EW
19	“Chuetsu-oki_Japan”	2007	Matsushiro Tokamachi	6.8	RSN4843_CHUETSU_65006NS/EW
20	“Chuetsu-oki_Japan”	2007	Joetsu Ogataku	6.8	RSN4848_CHUETSU_65011NS/EW
21	“Chuetsu-oki_Japan”	2007	Sawa Mizuguti Tokamachi	6.8	RSN4872_CHUETSU_65053NS/EW
22	“Iwate_Japan”	2008	“Yuzawa Town”	6.9	RSN5806_IWATE_55461NS/EW
23	“Iwate_Japan”	2008	“Kami_Miyagi Miyazaki City”	6.9	RSN5776_IWATE_54010NS/EW
24	“Darfield_New Zealand”	2010	“SPFS”	7	RSN6971_DARFIELD_SPFSN17E/73W
25	“Christchurch_New Zealand”	2011	“MQZ”	6.2	RSN8110_CCHURCH_MQZE/ZN

The target response spectrum for selected ground motions with a damping ratio of 4% is shown in Figure 9, where the similar acceleration response spectrum and average value of ground motions demonstrates the accuracy of the operation.

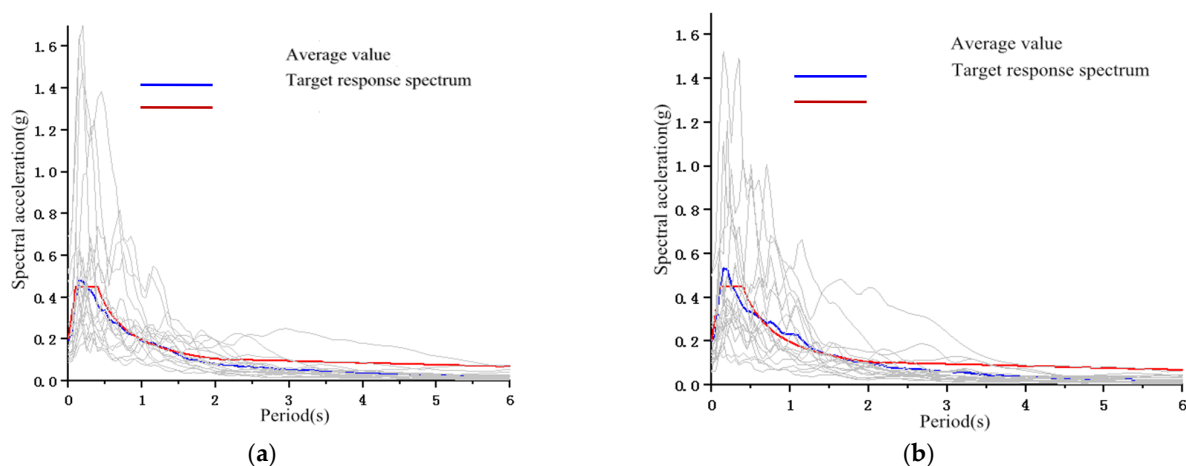


**Figure 9.** Response spectra of the selected ground motion records. (a) Horizontal component, N, and (b) horizontal component, E.

### 3.2. Selection of IM and DM

The peak ground acceleration (PGA), the peak ground velocity (PGV), and the spectral acceleration value (Sa) are often used as the intensity measures (IM) of ground motions. The authors of [22] suggested that PGA is relatively superior, which is consistent with the current seismic code in China. The peak inter-story drift ratio limit ( $\theta_{max}$ ) has the advantages of simple calculation and convenient application, which is directly related to the deformation capacity of buildings, and  $\theta_{max}$  was selected as the quantitative limit of the structure under different performance levels in domestic and foreign specifications. In this paper, PGA was chosen as the IM and  $\theta_{max}$  was chosen as the demand measure (DM), and the PGA of the selected ground motions scaled from 0.1 g to 2.0 g, with an interval of 0.2 g.

According to ATC-40 and GB/T 24335-2009,  $\theta_{max}$  was selected as the damage state to classified the performance level, where slight damage, moderate damage, and extensive damage correspond to characteristic points of the pseudo-static frame test, and the characteristic points include the yield point, maximum load point, and ultimate load point [16,23]. When  $\theta_{max}$  is greater than 0.1, the structure is considered as collapsed or complete damage [24]. The  $\theta_{max}$  values of the damage state were obtained based on the statistical data and relevant specifications, as shown in Table 3.

**Table 3.** Inter-story drift ratio limits of damage state for the CFST frame structure.

Damage State	Slight Damage (LS1)	Moderate Damage (LS2)	Extensive Damage (LS3)	Complete Damage (LS4)
$\theta_{max}$	1/150	1/50	1/30	1/10

### 3.3. Analysis and Discussion of IDA Results

#### 3.3.1. IDA Curve Clusters of In-Plane Frame

Figure 10 shows the plane frame subjected to 1D ground motions. It was calculated that the  $\theta_{max}$  of the plane frame models obtained from OpenSees was on the third floor or the fourth floor. IDA curve clusters of the plane frame subjected to 1D ground motions are shown in Figure 11a,b. Figure 11c shows IDA curve clusters of the in-plane frame subjected to 50 1D ground motions. With the increase in PGA, the slope of each curve decreased gradually, but the monotone increasing phenomenon did not always occur, and part of the IDA curves had states including “softening” and “zigzagging”.

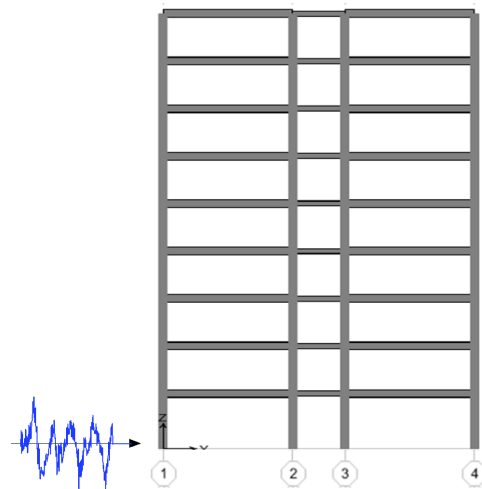


Figure 10. Plane frame subjected to 1D ground motions.

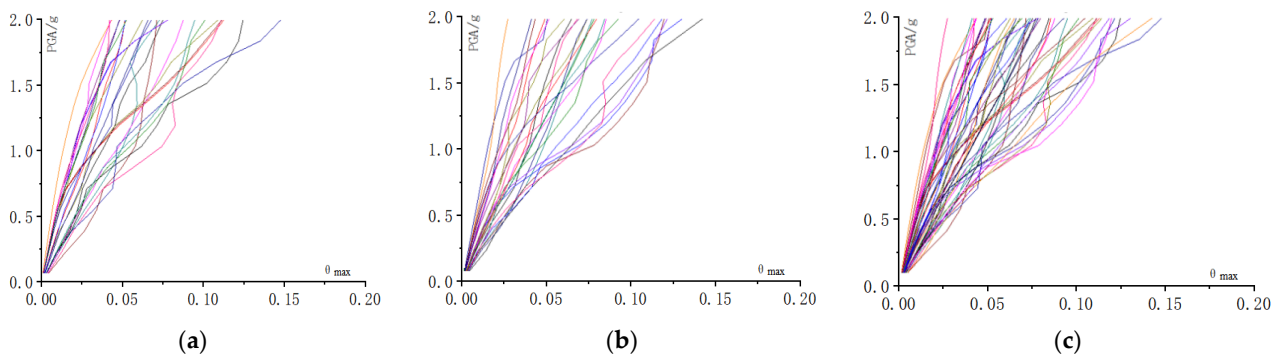


Figure 11. IDA curve clusters of the in-plane frame: (a) 25N, (b) 25E, and (c) 25N + 25E.

### 3.3.2. IDA Curve Clusters of Spatial Frame Subjected to 1D Ground Motions

Figure 12 shows the spatial frame subjected to 1D ground motions, and the weak axis direction (Y direction) of the spatial frame was taken as the main horizontal direction. IDA curve clusters of the spatial frame subjected to 1D ground motions are shown in Figure 13a–c. The comparison between Figures 11 and 13 showed that the difference between IDA curves of the spatial frame and plane frame for the same structural model subjected to 1D ground motions was significant. The average  $\theta_{max}$  of the spatial frame subjected to 1D ground motions was 10–20% larger than that of the plane frame. That is to say, the seismic response results of the plane frame were not enough to evaluate the seismic performance of the structure.

### 3.3.3. IDA Curve Clusters of Spatial Frame Subjected to 2D Ground Motions Considering Attacking Angle

Figure 14 shows the spatial frame subjected to 2D ground motions considering 13 attacking angles, where the angle  $\alpha$  is 0 to 180 degrees with the spacing of 15 degrees, while  $0^\circ$  represents the attacking angle of original ground motion. As shown in Figure 14, the black arrow line represents the attacking direction of the original ground motion, and the green arrow line represents the attacking direction of the ground motion at the angles of  $\alpha$ .

The inter-story drift ratios of each joint of the frame along the X and Y directions should be recorded, respectively, and then the  $\theta_{max}$  should be found by calculating according to the following formula:

$$\theta = \sqrt{\theta_x^2 + \theta_y^2} \quad (1)$$

where,  $\theta_x$  and  $\theta_y$  are inter-story drift ratios of any joint along the X and Y directions, respectively.

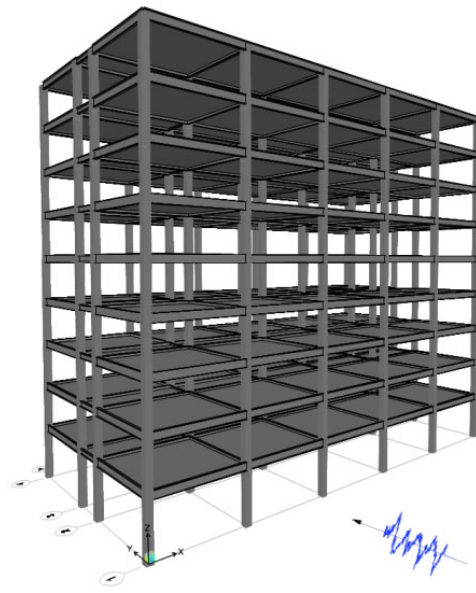


Figure 12. Spatial frame subjected to 1D ground motions.

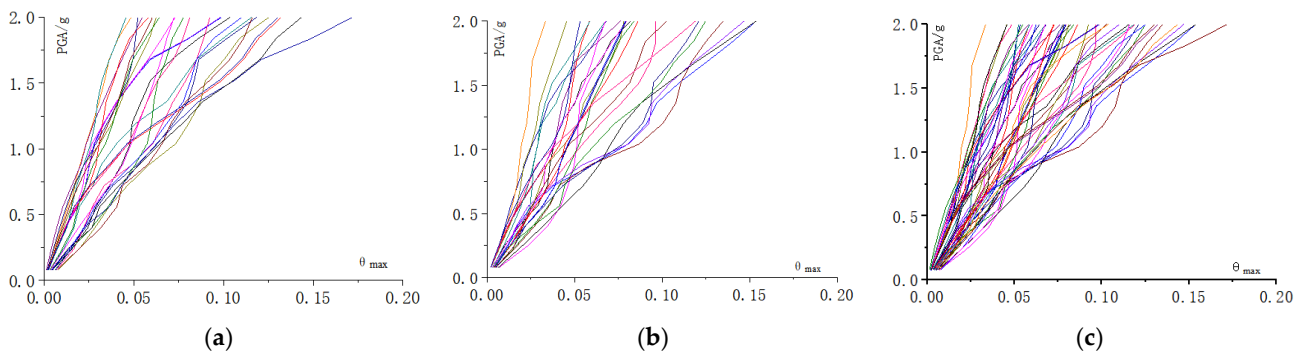


Figure 13. IDA curve clusters of the spatial frame subjected to 1D ground motions: (a) 25N, (b) 25E, and (c) 25N + 25E.

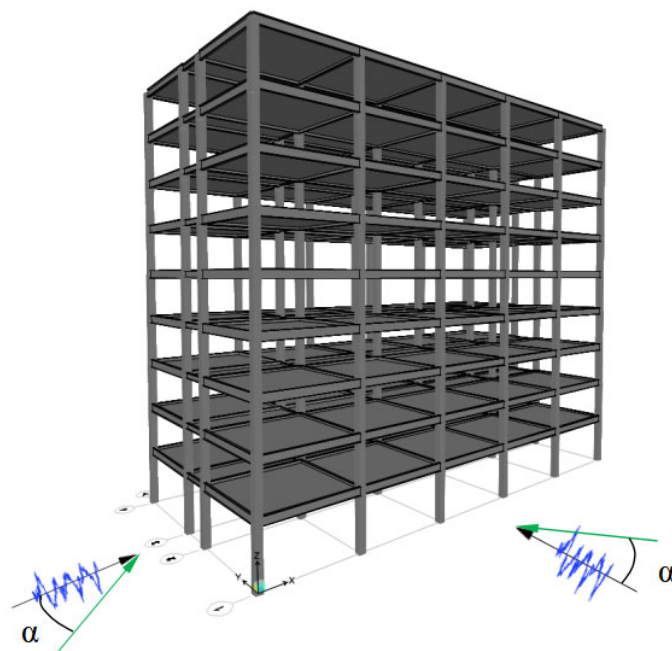
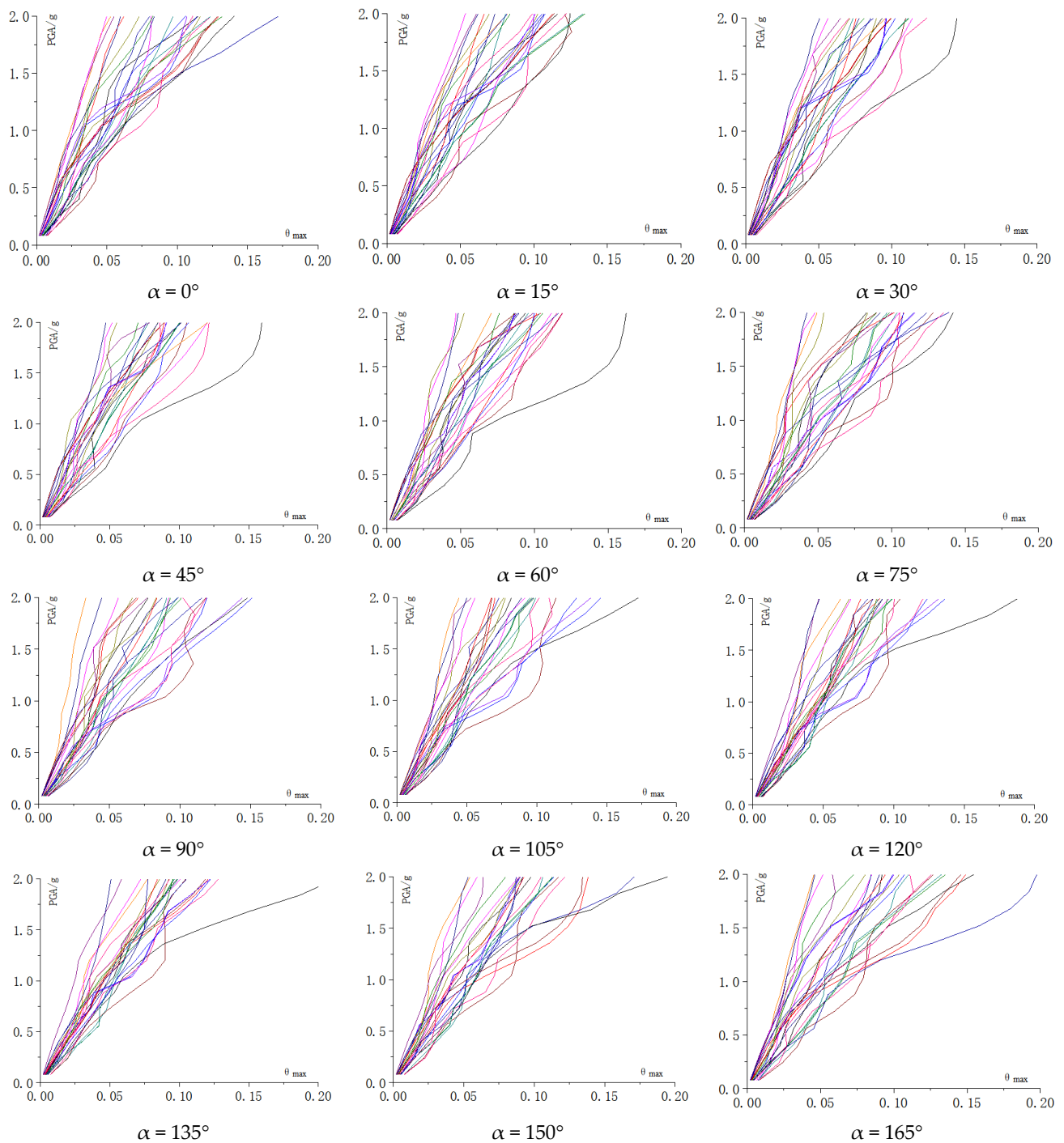


Figure 14. Spatial frame subjected to 2D ground motions considering the attacking angle.

The magnitude of peak acceleration will not completely determine the seismic response of the spatial frame, while the structural properties of the weak axis direction and the strong axis direction, the discount coefficient of the second horizontal component of ground motion, and the coupling effects in the two axis directions all affect the calculation results. By transforming the attacking angle of the ground motions, the sample of ground motion was greatly increased. IDA clusters of the spatial frame subjected to 2D ground motions under the different attacking angles are listed in Figure 15.



**Figure 15.** IDA curve clusters of the spatial frame subjected to 2D ground motions with different attacking angles.

In order to understand the influence of the attacking angle of ground motion on the  $\theta_{max}$  of the frame, the average value of  $\theta_{max}$  corresponding to each group of different attacking angles was used to compare the baseline of  $\bar{\theta}_{max,\alpha=0^\circ}$  in Figure 16. A certain trend can be found: When the attacking angle was  $15^\circ\text{--}45^\circ$ , there was little difference between  $\bar{\theta}_{max}$  and  $\theta_{max,\alpha=0^\circ}$ . When the attacking angle was  $60^\circ\text{--}120^\circ$ ,  $\text{PGA} < 1.5\text{ g}$ , the value of  $\bar{\theta}_{max}$  was greater than that of  $\theta_{max,\alpha=0^\circ}$ . When  $\text{PGA} > 1.5\text{ g}$ ,  $\bar{\theta}_{max}$  was less than  $\theta_{max,\alpha=0^\circ}$ . At the attacking angles of  $135^\circ$ ,  $150^\circ$ , and  $165^\circ$ , all the values of  $\bar{\theta}_{max}$  were greater than that of  $\bar{\theta}_{max,\alpha=0^\circ}$ . When  $\text{PGA} = 0.75\text{ g}$ , the difference between  $\bar{\theta}_{max}$  and  $\bar{\theta}_{max,\alpha=0^\circ}$  was the largest. The value of  $\theta_{max,\alpha=180^\circ}$  coincided almost exactly with that of  $\bar{\theta}_{max,\alpha=0^\circ}$ . In general, the seismic response was found to be sensitive to the attacking angle of ground motion.

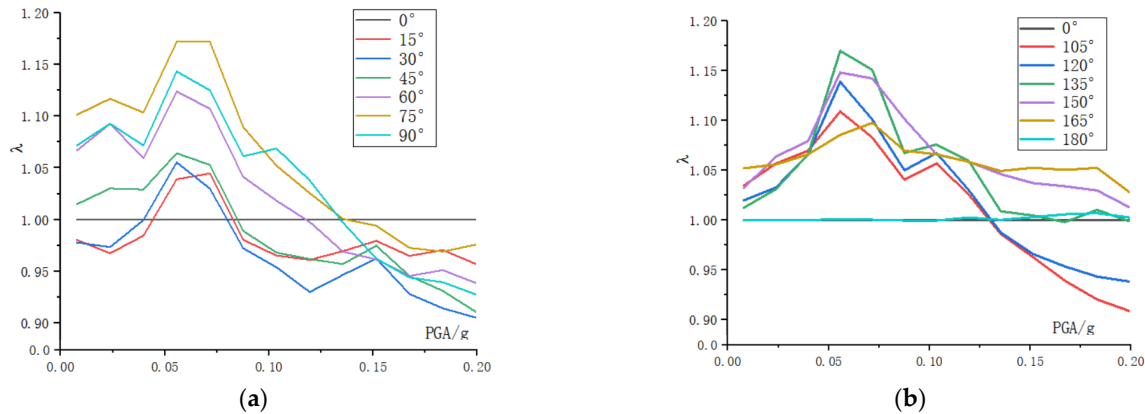


Figure 16. Comparison of  $\bar{\theta}_{max}$  of different attacking angles: (a)  $0^\circ\text{--}90^\circ$  and (b)  $105^\circ\text{--}180^\circ$ .

#### 4. Seismic Fragility Analysis

##### 4.1. Probabilistic Seismic Demand Model (PSDM)

IDA curves in Section 3 were used to establish the probabilistic seismic demand model between DM and IM. The regression formulas between PGA and  $\theta_{max}$  can be expressed as follows:

$$\ln(\theta_{max}) = a\ln(\text{PGA}) + b \tag{2}$$

where a and b are regression parameters.

According to the linear regression formula above, the regressions of the PSDM of CFST frames are listed in Table 4. The PSDMs of the plane frame, spatial frame subjected to 1D ground motions, and spatial frame subjected to 2D ground motions were quite different, and the PSDM of spatial frame was also different under different attacking angles.

Table 4. The fitting formula between  $\theta_{max}$  and PGA.

Structure	Ground Motions	Attacking Angle	The Linear Regression Formula
Plane frame subjected to 1D ground motions	25(N)	$0^\circ$	$\ln(\text{EDP}) = 1.133238\ln(\text{IM}) - 3.69704$
	25(E)	$0^\circ$	$\ln(\text{EDP}) = 1.093857\ln(\text{IM}) - 3.599816$
	50(25N + 25E)	$0^\circ$	$\ln(\text{EDP}) = 1.113548\ln(\text{IM}) - 3.648429$
Spatial frame subjected to 1D ground motions	25(N)	$0^\circ$	$\ln(\text{EDP}) = 1.015568\ln(\text{IM}) - 3.445141$
	25(E)	$0^\circ$	$\ln(\text{EDP}) = 0.9599472\ln(\text{IM}) - 3.364997$
	50(25N + 25E)	$0^\circ$	$\ln(\text{EDP}) = 0.9875820\ln(\text{IM}) - 3.405069$
Spatial frame subjected to 2D ground motions	25N + 25E	$0^\circ$	$\ln(\text{EDP}) = 1.011276\ln(\text{IM}) - 3.343988$
	25N + 25E	$15^\circ$	$\ln(\text{EDP}) = 1.006654\ln(\text{IM}) - 3.356569$
	25N + 25E	$30^\circ$	$\ln(\text{EDP}) = 0.986977\ln(\text{IM}) - 3.37602$
	25N + 25E	$45^\circ$	$\ln(\text{EDP}) = 0.975368\ln(\text{IM}) - 3.354419$
	25N + 25E	$60^\circ$	$\ln(\text{EDP}) = 0.958666\ln(\text{IM}) - 3.321175$
	25N + 25E	$75^\circ$	$\ln(\text{EDP}) = 0.952800\ln(\text{IM}) - 3.293288$
	25N + 25E	$90^\circ$	$\ln(\text{EDP}) = 0.946490\ln(\text{IM}) - 3.317331$
	25N + 25E	$105^\circ$	$\ln(\text{EDP}) = 0.958472\ln(\text{IM}) - 3.328774$

Table 4. Cont.

Structure	Ground Motions	Attacking Angle	The Linear Regression Formula
Spatial frame subjected to 2D ground motions	25N + 25E	120°	$\ln(\text{EDP}) = 0.973446\ln(\text{IM}) - 3.310517$
	25N + 25E	135°	$\ln(\text{EDP}) = 0.995960\ln(\text{IM}) - 3.275722$
	25N + 25E	150°	$\ln(\text{EDP}) = 0.995817\ln(\text{IM}) - 3.273766$
	25N + 25E	165°	$\ln(\text{EDP}) = 1.001221\ln(\text{IM}) - 3.295428$
	25N + 25E	180°	$\ln(\text{EDP}) = 1.012651\ln(\text{IM}) - 3.342390$
	(25N + 25E) × 13	All	$\ln(\text{EDP}) = 0.981602\ln(\text{IM}) - 3.32366$

#### 4.2. Seismic Fragility Curves

Seismic fragility analysis is the probability that the seismic response of a building will reach or exceed a certain performance level limit under different seismic effects. When  $IM = a$ , the exceeding probability exceeding the limit state value,  $C$ , is expressed as follows:

$$F(a) = P(\text{DM} \geq C / IM = a) \quad (3)$$

Therefore,  $F(a)$  can be then calculated according to Equation (3), according to the relationship between  $IM$  and  $DM$ :

$$F(a) = P(\text{DM} > C / IM = a) = \Phi \left[ \frac{\ln(\overline{\text{DM}}/C)}{\sqrt{\beta_{EDP}^2 + \beta_c^2}} \right] \quad (4)$$

where,  $\beta_{DM}$  and  $\beta_C$  are the logarithmic standard deviation of the structural seismic response and critical value of failure state, respectively. The value of  $\sqrt{\beta_{DM}^2 + \beta_c^2}$  is related to the seismic intensity index, the spectral acceleration was 0.4, and the peak acceleration was 0.5 [22]. The exceeding probability curve can be further obtained from the equation, which is the fragility curve, and the curve transitions from steep to gradual as the damage progresses from slight damage to near collapse.

#### 4.3. Effect of the Attacking Angle on Seismic Fragility

Figure 17 presents the comparison of seismic fragility curves between different attacking angles and 0° (original attacking angle).

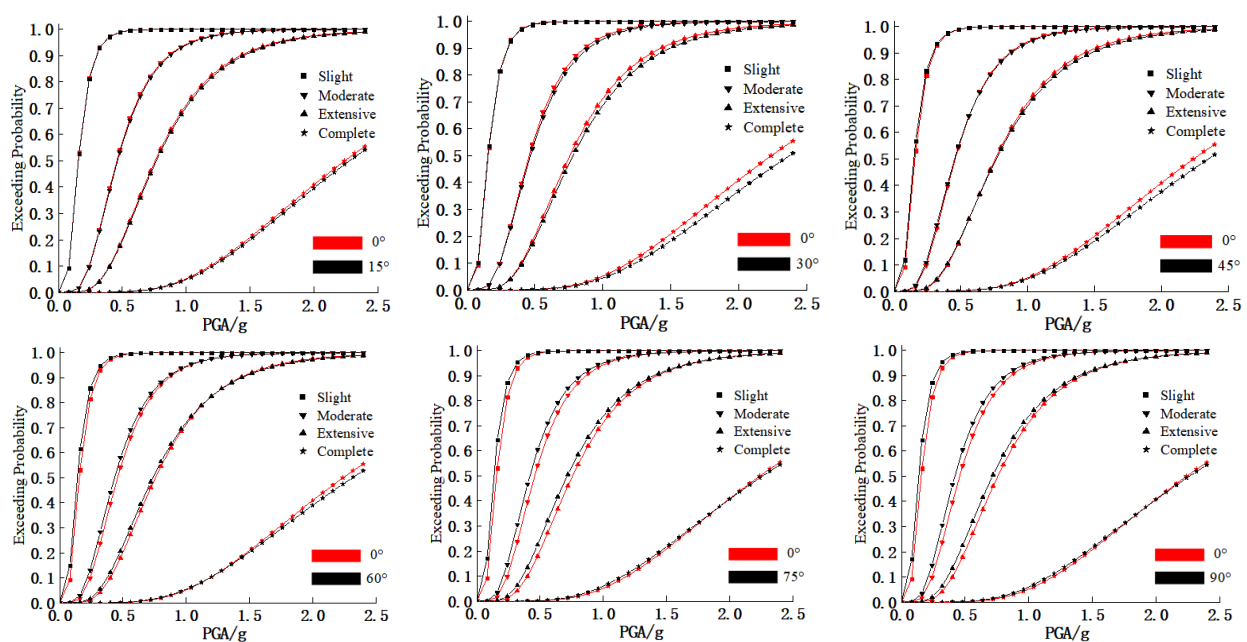
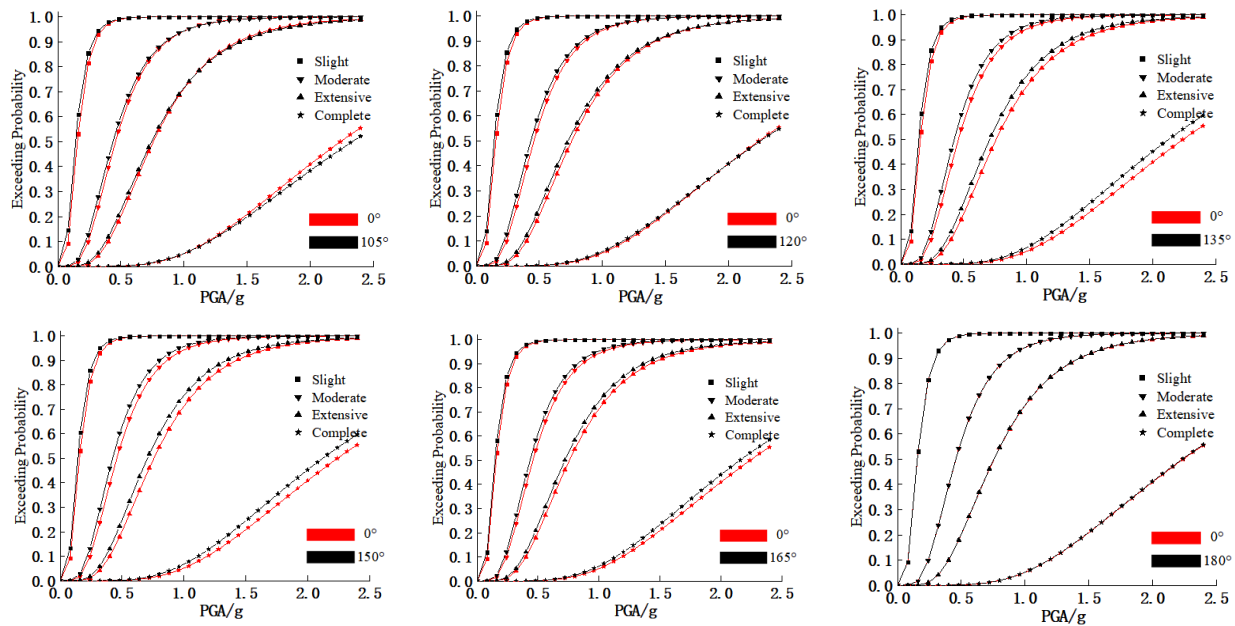


Figure 17. Cont.



**Figure 17.** Seismic fragility curves of the spatial frame subjected 2D ground motions of different attacking angles.

When the attacking angle was 15–45°, the exceeding probability of fragility curves at the three performance levels (LS1–LS3) was close to that of the 0° fragility curves, and the exceeding probability of the 0° fragility curves in LS4 was larger than that of the others. When the attacking angle was 60–90°, the exceeding probability of fragility curves at the three performance levels (LS1–LS3) was larger than that of the 0° fragility curves, while the exceeding probability was close to that of the 0° fragility curves in LS4. The exceeding probability of the 135°, 150°, and 165° fragility curves was larger than that of the 0° fragility curves at each performance level. The 180° fragility curve coincided perfectly with the 0° fragility curves. In general, the exceeding probability was found to be sensitive to the attacking angle of ground motion, and the seismic fragility analysis did not only focus on the original attacking angle, but also considered the adverse effects of different attacking angles.

#### 4.4. The Comparison of Fragility Analysis Curves of CFST Plane Frame and Spatial Frame

The comparison of fragility analysis curves is shown in Figure 18. The red line represents the seismic fragility analysis results of the in-plane frame subjected to 1D ground motions (25N + 25E) at 10 intensities, so that, in total, 500 (=50 × 10) nonlinear dynamic analyses were performed. The black line represents the seismic fragility analysis results of the spatial frame subjected to 1D ground motions (25N + 25E) at 10 intensities, in a total of 500 (=50 × 10) analyzed cases. The blue line represents the seismic fragility analysis results of the spatial frame subjected to 2D ground motions (25N + 25E) at 10 intensities considering 13 attacking angles, in a total of 3250 (=25 × 10 × 13) analyzed cases.

At the LS1 level, the fragility curves of the spatial frame subjected 2D ground motions and 1D ground motions almost coincided, and the exceeding probability of the spatial frame was larger than that of the plane frame. At the level of damage state from LS1 to near collapse, the fragility curves showed obvious characteristics. The exceeding probability of the spatial frame subjected to 2D ground motions at each performance level was successively greater than that of the 1D ground motion, and greater than that of the plane frame. This shows that for 2D earthquakes, it is easier to motivate the frame structure to exceed a certain damage state. As shown in Tables 5 and 6, when the structure was under the intensity level of frequent earthquakes (PGA = 0.2 g), the exceeding probability of the spatial frame subjected to 2D ground motions was close to 73% in the slight damage

state, while the exceeding probability of the plane frame was close to 59%. In the moderate damage state, the exceeding probability of spatial frame subjected to 2D ground motions was 50% higher than that of the plane frame. When PGA = 0.3 g, the exceeding probability of spatial frame was 10% higher than that of plane frame. In addition, from LS2 to near LS4, the difference in seismic fragility curves was gradually enlarged. This shows that the spatial frame subjected to 2D ground motions is more likely to cause more severe damage to the structure under a large earthquake intensity. Therefore, when the IDA-based seismic fragility method is employed to evaluate the seismic performance of the CFST frame structure, it is necessary to adopt the spatial frame and consider bidirectional inputs of ground motions.

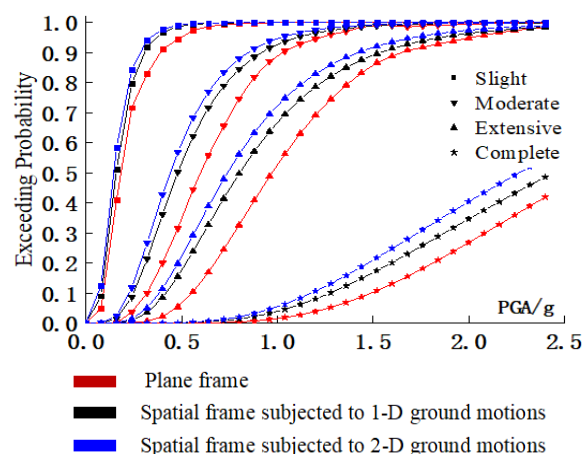


**Figure 18.** Fragility analysis curves of the CFST plane frame and spatial frame.

**Table 5.** The exceeding probabilities of the CFST frame under PGA of 0.2 g.

	Damage State			
	LS1	LS2	LS3	LS4
Plane frame	0.586	0.019	0.002	0
Spatial frame subjected to 1D ground motions	0.667	0.051	0.005	0
Spatial frame subjected to 2D ground motions	0.735	0.072	0.008	0

**Table 6.** The exceeding probabilities of the CFST frame under PGA of 0.3 g.

	Damage State			
	LS1	LS2	LS3	LS4
Plane frame	0.806	0.083	0.004	0
Spatial frame subjected to 1D ground motions	0.890	0.182	0.0285	0
Spatial frame subjected to 2D ground motions	0.919	0.228	0.0416	0

## 5. Conclusions

In this paper, we conducted seismic fragility analysis of a nine-story CFST plane frame and spatial frame employing the IDA method. Based on the analysis results, the following conclusions can be summarized:

- (1) For the CFST spatial frame under 2D ground motions, the seismic fragility analysis result was found to be sensitive to the attacking angle of ground motion, where the exceeding probability of the 15°, 30°, and 45° fragility curves at the levels LS1–LS3 was close to that of the 0° fragility curves, the exceeding probability of the 60°–90° fragility curves at the levels LS1–LS3 was larger than that of the 0° fragility curves, and the exceeding probability of the 135°, 150°, and 165° fragility curves was larger than that of the 0° fragility curves at each performance level.

- (2) The results of the seismic fragility analysis of the spatial frame were obviously different from those of the plane frame. The analytical results showed that the exceeding probability of the spatial frame under 2D ground motions was successively greater than that under 1D ground motions, and greater than the plane frame, and the maximum difference at each performance level was up to 6% and 16%, respectively.
- (3) IDA-based seismic fragility analysis of CFST frames should adopt the spatial frame model and consider the effect of the attacking angle of 2D ground motions, rather than the plane frame model.

**Author Contributions:** C.X. established the structure model and analyzed the data; X.L. analyzed the data and wrote the paper. All authors have read and agreed to the published version of the manuscript.

**Funding:** The authors appreciate the financial support granted by the National Natural Science Foundation of China (Grant No. 51678457).

**Data Availability Statement:** The original contributions presented in the study are included in the article, further inquiries can be directed to the corresponding author.

**Conflicts of Interest:** The authors declare that they have no known competing financial interests or personal relationships that could have appeared to influence the work reported in this paper.

## References

1. Cheng, Y.; Dong, Y.-R.; Bai, G.-L.; Wang, Y.-Y. IDA-based seismic fragility of high-rise frame-core tube structure subjected to multi-dimensional long-period ground motions. *J. Build. Eng.* **2021**, *43*, 102917. [[CrossRef](#)]
2. Rajkumari, S.; Thakkar, K.; Goyal, H. Fragility analysis of structures subjected to seismic excitation: A state-of-the-art review. *Structures* **2022**, *40*, 303–316. [[CrossRef](#)]
3. Wang, J.; Sun, Y. Seismic fragility and post-earthquake reparability of concrete frame with low-bond high-strength reinforced concrete column. *Structures* **2022**, *37*, 185–202. [[CrossRef](#)]
4. Rezaei, H.; Zarfam, P.; Golafshani, E.M.; Amiri, G.G. Seismic fragility analysis of RC box-girder bridges based on symbolic regression method. *Structures* **2022**, *38*, 306–322. [[CrossRef](#)]
5. Jia, D.-W.; Wu, Z.-Y. Seismic fragility analysis of RC frame-shear wall structure under multidimensional performance limit state based on ensemble neural network. *Eng. Struct.* **2021**, *246*, 112975. [[CrossRef](#)]
6. Bao, C.; Ma, X.; Lim, K.S.; Chen, G.; Xu, F.; Tan, F.; Hamid, N.H.A. Seismic fragility analysis of steel moment-resisting frame structure with differential settlement. *Soil Dyn. Earthq. Eng.* **2021**, *141*, 106526. [[CrossRef](#)]
7. Xu, C.; Guo, C.; Xu, Q.; Yang, Z. The global collapse resistance capacity of a seismic-damaged SRC frame strengthened with an enveloped steel jacket. *Structures* **2021**, *33*, 3433–3442. [[CrossRef](#)]
8. Vasileiadis, V.; Kostinakis, K.; Athanatopoulou, A. Story-wise assessment of seismic behavior and fragility analysis of R/C frames considering the effect of masonry infills. *Soil Dyn. Earthq. Eng.* **2023**, *165*, 107714. [[CrossRef](#)]
9. Mansouri, I.; Hu, J.W.; Shakeri, K.; Shahbazi, S.; Nouri, B. Assessment of seismic vulnerability of steel and RC moment buildings using HAZUS and statistical methodologies. *Discret. Dyn. Nat. Soc.* **2017**, *2017*, 2698932. [[CrossRef](#)]
10. Qu, Z.; Ye, L.; Pan, P. Comparative study on methods of selecting earthquake ground motions for nonlinear time history analyses of building structures. *China Civ. Eng. J.* **2011**, *44*, 10–21.
11. Yang, F.; Gao, X.; Zhang, W. Response of tall-building steel structure to multi-dimensional seismic action. *J. Build. Struct.* **2003**, *24*, 33–43.
12. Kostinakis, K.; Morfidis, K.; Xenidis, H. Damage response of multistorey r/c buildings with different structural systems subjected to seismic motion of arbitrary orientation. *Earthq. Eng. Struct. Dyn.* **2015**, *44*, 1919–1937. [[CrossRef](#)]
13. Lagaros, N.D. Multicomponent incremental dynamic analysis considering variable incident angle. *Struct. Infrastruct. Eng.* **2010**, *6*, 77–94. [[CrossRef](#)]
14. GB50936-2014; Technical Code for Concrete Filled Steel Tubular Structures. Ministry of Housing and Urban-Rural Development of the People's Republic of China: Beijing, China, 2014.
15. JGJ138-2016; Code for the Design of Composite Structures. Ministry of Housing and Urban-Rural Development of the People's Republic of China: Beijing, China, 2016.
16. Liu, X.; Xu, C.; Peng, S.; Zhou, B. Influence of staggered floor and unequal height of left and right beam on seismic behavior of CFSST column-to-HSS beam composite frames. *J. Build. Eng.* **2023**, *66*, 105878. [[CrossRef](#)]
17. Wang, K.; Lu, X.-F.; Yuan, S.-F.; Cao, D.-F.; Chen, Z.-X. Analysis on hysteretic behavior of composite frames with concrete-encased CFST columns. *J. Constr. Steel Res.* **2017**, *135*, 176–186. [[CrossRef](#)]
18. Zhang, Z.; Wang, J.; Li, B.; Zhao, C. Seismic tests and numerical investigation of blind-bolted moment CFST frames infilled with thin-walled SPSWs. *Thin Walled Struct.* **2019**, *134*, 347–362. [[CrossRef](#)]

19. Chen, J.; Bian, Y.; Su, L. Application of OpenSees on calculating lateral force-displacement hysteretic curves of concrete-filled steel tubular frame with unequal spans. *World Earthq. Eng.* **2021**, *37*, 111–118.
20. Xu, C.; Deng, J.; Peng, S.; Li, C. Seismic fragility analysis of steel reinforced concrete frame structures based on different engineering demand parameters. *J. Build. Eng.* **2018**, *20*, 736–749. [[CrossRef](#)]
21. *GB/T50011-2010*; Code for Seismic Design of Buildings. Ministry of Housing and Urban-Rural Development of the People's Republic of China: Beijing, China, 2024.
22. Karafagka, S.; Fotopoulou, S.; Pitilakis, D. Fragility assessment of non-ductile RC frame buildings exposed to combined ground shaking and soil liquefaction considering SSI. *Eng. Struct.* **2021**, *229*, 111629. [[CrossRef](#)]
23. *Research on Seismic Behavior and Design Method of Composite Frame with Reinforced Concrete Columns and Steel Beams*; Xi'an University of Architecture and Technology: Xi'an, China, 2014.
24. Jalali, S.A.; Amini, A.; Mansouri, I.; Hu, J.W. Seismic collapse assessment of steel plate shear walls considering the mainshock–aftershock effects. *J. Constr. Steel Res.* **2021**, *182*, 106688. [[CrossRef](#)]

**Disclaimer/Publisher's Note:** The statements, opinions and data contained in all publications are solely those of the individual author(s) and contributor(s) and not of MDPI and/or the editor(s). MDPI and/or the editor(s) disclaim responsibility for any injury to people or property resulting from any ideas, methods, instructions or products referred to in the content.